ACS APPLIED MATERIALS & INTERFACES

Research Article

Cite This: ACS Appl. Mater. Interfaces 2019, 11, 29978−29984

www.acsami.org

Interfacial Molecule Mediators in Cathodes for Advanced Li−S Batteries

Yuchong Lai, Huagui Nie, Xiangju Xu, Guoyong Fang, Xinwei Ding, Dan Chan, Suya Zhou, Yonggui Zhang, Xi'an Chen, and Zhi Yang*

Key Laboratory of Carbon Materials of Zhejiang Province, College of Chemistry and Materials Engineering, Wenzhou University, Wenzhou 325035, PR China

Supporting Information

ABSTRACT: The complicated reactions at the cathode−electrolyte interface in Li−S batteries are a large barrier for their successful commercialization. Herein, we developed a molecular design strategy and employed three small molecules acting as interfacial mediators to the cathodes of Li−S batteries. The theoretical calculation results show that the incorporation of tris(4-fluorophenyl)phosphine (TFPP) has a strong binding performance. The experimental results demonstrate that the strong chemical interactions between polysulfides and the F, P atoms in TFPP not only modify the kinetics of the electrochemical processes in the electrolyte but also promote the formation of short-chain clusters (Li_2S_x, x = 1, 2, 3, and 4) at the interface during the charge−discharge process. As a result, an optimized electrode exhibits a low capacity decay rate of 0.042% per cycle when the current rate is increased to 5 C over 1000 cycles.

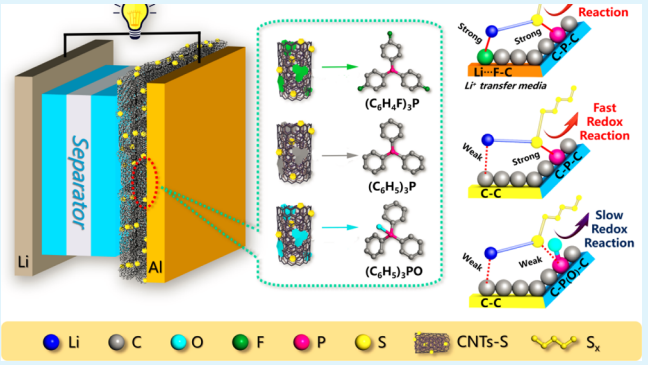

KEYWORDS: *Li−S batteries, interfacial mediate, molecule mediator, tris(4-fluorophenyl)phosphine, polysulfide*

1. INTRODUCTION

Lithium−sulfur (Li−S) batteries are regarded as one of the most promising energy storage devices for next-generation batteries, owing to their high specific energy (2600 W h kg^{-1}) and superior theoretical specific capacity (1675 mA h g^{-1})[1−3] Despite these considerable advantages, practical applications of rechargeable Li−S batteries remain a challenge as a result of several issues. These include the low electrical conductivity of sulfur and its solid discharging products (Li_2S or Li_2S_2), the shuttle effect associated with soluble intermediate polysulfides (LiPSs), and the volume expansion of sulfur upon lithiation[4−8] Many strategies have been proposed to mitigate these challenges, including conductive host substances[7,9−16] (e.g., porous carbon nanotube, doped graphene) and specific inorganic anchoring materials[1,17−23] (e.g., TiO_2, CoS_2, Ti_3C_2 MXene nanoribbon, and V_2O_5). These approaches have improved the capacity and cycling stability of Li−S batteries to a large extent. Even so, the use of these batteries in actual electric vehicles or large-scale energy storage systems requires both the overall sulfur content in the batteries and the overall sulfur-loading area to be significantly increased, which in turn leads to an increased shuttle effect, slow redox kinetics, and more undesirable side reactions.[6,24,25] Especially the complicated reactions at the cathode−electrolyte interface are still a large barrier for the successful commercialization of Li−S batteries.[5,26,27] Recently, various sophisticated strategies[28−32] have been researched with the aim of efficiently promoting battery reactions without lowering the overall energy density. Wen and co-workers[33,34] discovered that mediation at the cathode−electrolyte interface by Li salts reduces the overpotential, lowers the internal resistance associated with Li−S redox reactions, and increases the energy density of Li−S batteries. Zhang et al.[35] developed a cooperative interface based on "sulfiphilic" Ni−Fe-layered double hydroxides and "lithiophilic" nitrogen-doped graphene as a means of enhancing the retention of LiPSs and promoting the formation of Li_2S. Introducing various interfacial mediators into the cathodes of Li−S systems has become a popular strategy. However, considering the complexity of these mediator compositions and their uncertain molecular structural characteristics on the atomic scale, it is difficult to obtain an in-depth understanding of the mediating mechanism as well as the structure−performance relationship.

In the present work, we developed a molecular design strategy and employed a series of small molecules with specific structures, including tris(4-fluorophenyl)phosphine (TFPP), triphenylphosphine (TPP), and triphenylphosphine oxide (TPPO), as interfacial mediators in cathodes for Li−S systems. The theoretical calculation results show that the incorporated TFPP has the strongest binding performance among the three

Received: June 8, 2019
Accepted: July 30, 2019
Published: July 30, 2019

DOI: 10.1021/acsami.9b10049
ACS Appl. Mater. Interfaces 2019, 11, 29978−29984

small molecules. The electrochemical impedance spectroscopy (EIS) and in situ UV−visible spectroscopy data together with other experimental results demonstrate that the strong chemical interactions between LiPSs and the F, P atoms in TFPP not only modify the kinetics of the electrochemical processes in the electrolyte, but also promote the formation of short-chain clusters (Li_2S_x, x = 1, 2, 3, and 4) at the interface during the charge−discharge process. As a result, an optimized electrode exhibits a low capacity decay rate of 0.042% per cycle when the current rate is increased to 5 C over 1000 cycles. Additionally, upon increasing the sulfur loading area to 4.2 mg cm^{-2}, the battery maintains a much higher discharge capacity of 549 mA h g^{-1} after 140 cycles.

2. RESULT AND DISCUSSION

A schematic illustration of the battery configuration is presented in Figure 1. In contrast to previously reported

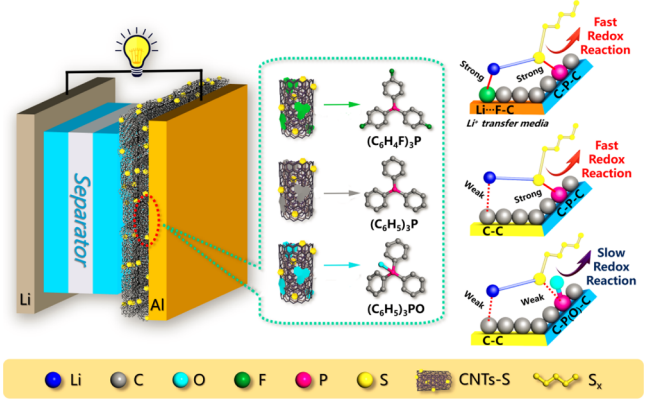

Figure 1. Schematic of electrode configuration for Li−S battery with TFPP, TPP, and TPPO.

CNTs/S cathodes,[12,17,36] our work employed a design based on three electrodes with small molecules (TFPP, TPP, and TPPO) that adhered to the surface of carbon nanotubes (CNTs) as mediators via $\pi-\pi$ stacking interactions. The resulting cathodes are referred to herein as CNTs/S/TFPP, CNTs/S/TPP, and CNTs/S/TPPO, respectively. Standard 2025 coin cells were assembled using a cathode with the mediator versus a metallic lithium anode (details of the experiments are provided in the Experimental Section in the Supporting Information). For comparison, a cell using a CNTs/sulfur cathode without a mediator was also fabricated and is referred to as the CNTs/S specimen. The rate performances of CNTs/S/TFPP cathodes with different mass ratio of TFPP are summarized in Figure S1. A TFPP level of 5 wt % evidently shows the highest discharge capacity at various rates. For this reason, all CNTs/S/TFPP cathode materials used in subsequent work contained 5 wt % TFPP unless otherwise noted.

Cycle voltammetry (CV) plots obtained from the CNTs/S/TFPP, CNTs/S/TPP, CNTs/S/TPPO, and CNTs/S cathodes over the initial four cycles are presented in Figures 2A and S2. It can be seen that CNTs/S/TFPP and CNTs/S/TPP had more positive onset potentials during the reduction process compared with CNTs/S/TPPO and CNTs/S. Table S1 summarizes the voltage hysteresis (ΔV) and I_{pa}/I_{pc} (where I_{pa} and I_{pc} are the oxidative and reductive peak currents, respectively) values derived from the CV data. Compared with CNTs/S/TPP, CNTs/S, and CNTs/S/TPPO, the CNTs/S/TFPP cathode generated the lowest ΔV and its I_{pa}/I_{pc} value was closest to 1.[37] These results suggest low internal resistance, high reversibility, and rapid conversion of polysulfides in this CNTs/S/TFPP cell. Figure 2B shows the rate performances of the CNTs/S/TFPP, CNTs/S/TPP, CNTs/S/TPPO, and CNTs/S cathodes over the range from 0.2 to 2 C (1 C = 1675 mA h g^{-1}). The Galvanostatic charge−discharge curves produced by the four cathodes at various current rates (0.2−2 C) are presented in Figures 2C,D and S3. Among the four cathodes, CNTs/S/TFPP delivered the highest discharge capacity at all rates. This cathode exhibited a high initial capacity of 1492 mA h g^{-1} at the rate of 0.2 C, which was reduced to 1041, 941, and 866 mA h g^{-1} when the rate was increased to 0.5, 1, and 2 C. In addition, the CNTs/S/TFPP cathode had the lowest degree of electrochemical polarization (i.e., the lowest voltage hysteresis, ΔE_v)[17] in its Galvanostatic charge−discharge curve (see Table S2), which is consistent with the polarized voltage value (ΔV) obtained from the CV data (Table S1).

Cycling stability is an important factor when assessing the performance of Li−S batteries, and the data acquired during prolonged cycling of CNTs/S/TFPP and CNTs/S at 1 C are summarized in Figure 2E. It is evident that the capacity of the CNTs/S/TFPP cell was always higher than that of CNTs/S at 1 C throughout the 400 cycles. When the current rate was increased to 5 C (Figure 2F), the CNTs/S/TFPP cathode still showed a capacity of 300 mA h g^{-1} after 1000 cycles, representing a low capacity decay rate of 0.042% per cycle. These data demonstrated excellent stability at a high current rate. In addition, a CNTs/S/TFPP cathode with a sulfur loading of 4.2 mg cm^{-2} was assembled and cycled. Figure 2G shows that the CNTs/S/TFPP cathode retained a capacity of 545 mA h g^{-1} after 140 cycles. Based on the high sulfur loading in related electrodes, the performance of CNTs/S/TFPP is comparable to those recently reported for other devices (Table S3). These results demonstrate the high performance of the CNTs/S/TFPP cathode, as well as its potential for practical applications.

EIS was employed to assess the interfaces in the various specimens, and Figure 3A−C shows the Nyquist curves for CNTs/S/TFPP, CNTs/S/TPP, and CNTs/S, respectively, as acquired at 2 C with different cycles. Based on the work by Liu et al.,[19,38] it is known that the profiles of the three cathodes, which exhibit one semicircle in the high-frequency zone, suggest charge-transfer resistance, whereas the other semicircle in the medium frequency range corresponds to a solid film composed of Li_2S and Li_2S_2. These curves were fitted as shown in Figure 3D.[19] According to the fitting results in Figure 3E, the charge-transfer resistance values (R_c) for the CNTs/S/TFPP, CNTs/S/TPP, and CNTs/S cathodes over the span of 5 to 500 cycles ranged from 10 to 20 Ω. In contrast, the interfacial resistance values (R_i) of the cathodes with mediators differed significantly from that for the standard cathode. The R_i values for the CNTs/S cathode also increased gradually from 5 to 500 cycles, whereas the values for CNTs/S/TFPP and CNTs/S/TPP became lower, especially that of CNTs/S/TFPP. It is evident that the cathodes with small molecule mediators accelerated the conversion reactions in the solid film composed of Li_2S and Li_2S_2, whereas reducing the amount of insulating products and mitigating interfacial deterioration during the charge−discharge process.[6,33,38] Obviously, these results indicate that enhanced redox kinetics and increased

DOI: 10.1021/acsami.9b10049
ACS Appl. Mater. Interfaces 2019, 11, 29978−29984

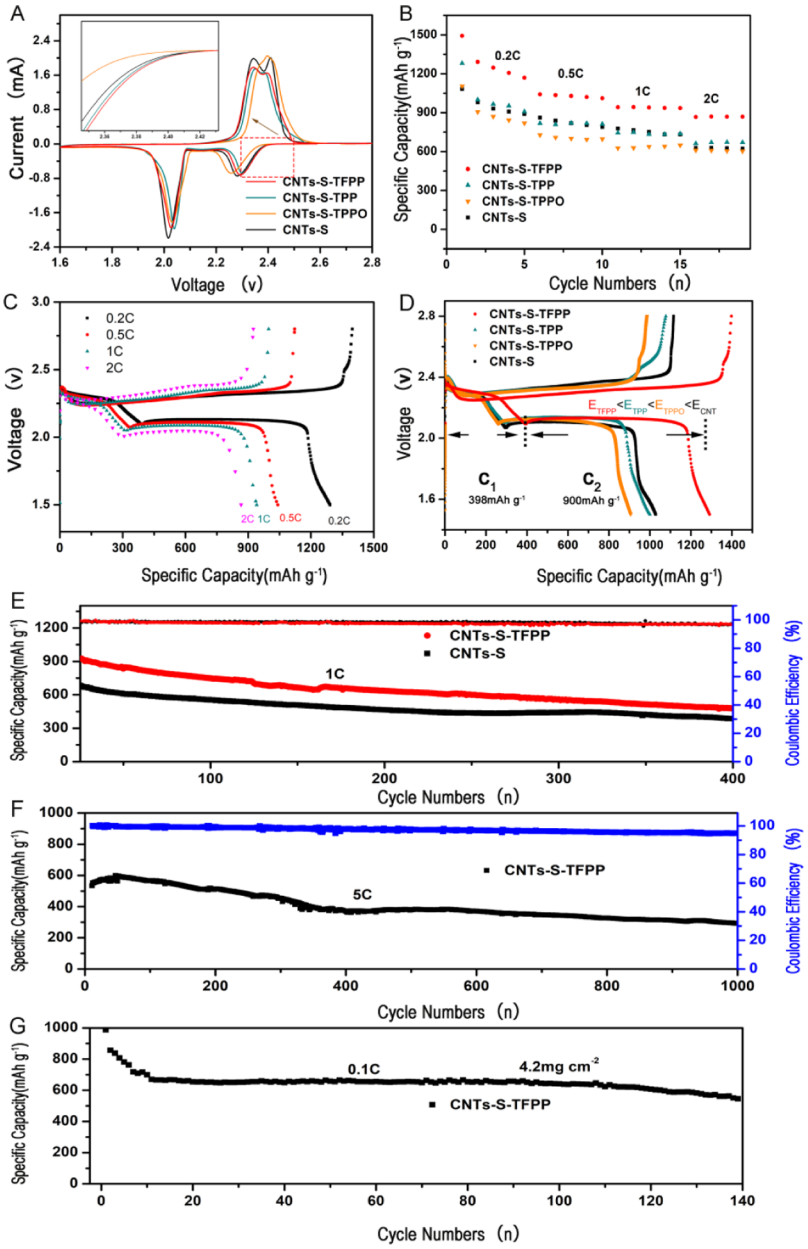

Figure 2. Electrochemical performances of CNTs/S/TFPP compared with CNTs/S/TPP, CNTs/S/TPPO, and CNTs/S. (A) Third cycle of CV profiles, (B) rate performance, (C) galvanostatic discharge−charge plots at various rates. (D) Galvanostatic discharge−charge plots at 0.2 C. (E) Cycling stability of CNTs/S/TFPP and CNTs/S cathode at 1 C. (F) Cycling performance of CNTs/S/TFPP cathode at 5 C. (G) Cycling stability of CNTs/S/TFPP with 4.2 mg cm^{-2} at 0.1 C.

reaction efficiency resulted from the use of TFPP as a mediator.[6]

The interfacial influence of F, Li, and S throughout the cathodes was further investigated by X-ray photoelectron spectroscopy (XPS). Considering the distraction of the poly(vinylidene fluoride) (Figure S3), the electrode binder was changed to sodium alginate ($C_6H_7O_6Na$) prior to acquiring the F 1s and Li 1s spectra. The high-resolution F 1s spectra acquired from the four electrodes after the cycles are shown in Figure 4A. It is evident that the spectrum produced by the CNTs/S/TFPP is different from those of the other three cathodes. In the case of the F 1s spectra, the peak generated by the CNTs/S/TFPP appears at 688.6 eV, indicating electron-acquisition behavior[39,40] and suggesting that there was a tendency to form F−Li bonds. In addition, the peak at 686.4 eV associated with LiF[39] in the CNTs/S/TFPP spectrum is almost nonexistent, meaning that the F−Li bonds in this system were different from those in typical LiF compounds. The Li spectrum (Figure 4B) contains a peak attributed to TFPP that has a distinct low-field shift, suggesting the existence of lithium bonds.[41−43]This result together with the EIS analyses above (Figure 3) confirms that the F in the TFPP undergoes strong chemical anchoring to LiPSs species to accelerate Li^+ transport between low-chain and high-chain sulfides at the interface, which in turn retards the degradation of the interface during cycling.[6,33,34]In the high-resolution S 2p spectra (Figure 4C), the S−P interaction peak appears at 163.9 eV[44] in the case of those cathodes having small molecules, and the peak produced by CNTs/S/TFPP is stronger than those generated by the other two cathodes with meditators (CNTs/

DOI: 10.1021/acsami.9b10049
ACS Appl. Mater. Interfaces 2019, 11, 29978−29984

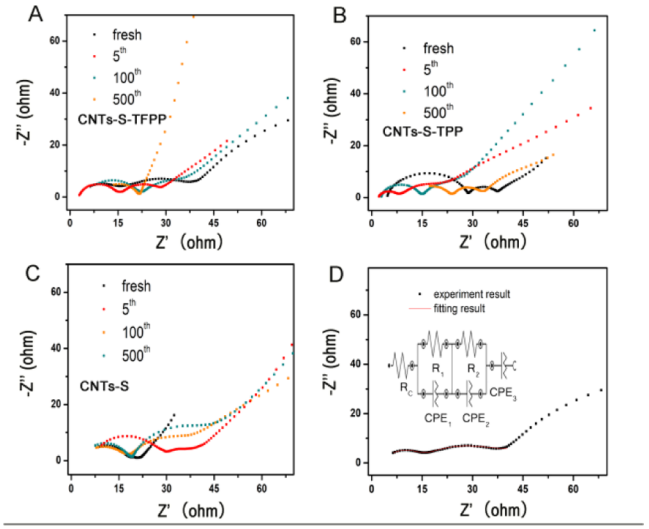

E Name	R_e(Ω)	R_c (Ω)	R_i (Ω)
CNTs-S-TFPP(fresh)	3.33	10.7	25.7
CNTs-S-TFPP(5th)	3.42	9.9	22.2
CNTs-S-TFPP(100th)	4.81	15.2	6.09
CNTs-S-TFPP(500th)	8.94	12.7	\
CNTs-S-TPP(fresh)	2.16	26.6	16.2
CNTs-S-TPP(5th)	2.35	10.3	21.6
CNTs-S-TPP(100th)	1.94	16.9	17.9
CNTs-S-TPP(500th)	11.5	10.6	5.3
CNTs-S (fresh)	0.3	11.2	1.26
CNTs-S(5th)	2.73	19.6	6.7
CNTs-S(100th)	2.58	12.7	8.99
CNTs-S(500th)	3.25	14.6	13.1

Figure 3. Study of the interfaces in the various specimens. The Nyquist plots of (A) CNTs/S/TFPP, (B) CNTs/S/TPP, and (C) CNTs/S; (D) Nyquist EIS and corresponding equivalent for CNTs/S/TFPP; (E) electrolyte resistance (R_e), the charge-transfer resistance (R_c), and the interface resistance (R_i) of the three cathodes.

S/TPP and CNTs/S/TPPO). These data suggest the presence of powerful S−P interactions in CNTs/S/TFPP, which may accelerate the catalytic conversion of polysulfides. To provide further evidence, the CNTs/S/TFPP, CNTs/S/TPP, and CNTs/S cathodes were employed to obtain CV data in H-shaped electrolytic cells. During these trials, the color of CNTs/S/TFPP in the right chamber, which was filled with a LiPSs solution, was observed to fade after 200 cycles (Figure S6). This result demonstrates that the mediator TFPP effectively converted the LiPSs and thus greatly suppressed the shuttle effect.[19]

It is important to study the reaction mechanisms of these units in depth, and so working electrodes were fabricated from CNTs with TFPP or TPP and pure CNTs without mediators. In situ UV−visible spectroscopy (Figure S6) was used to assess the CNTs, CNTs/TFPP, and CNTs/TPP electrodes in a Li_2S_8 solution during the discharge process. The data (Figure S7) showed that the primary reaction intermediates included S_8^{2-} (appearing at 560 nm), S_6^{2-} (475 nm), S_4^{2-} (420 nm), and $S_3^{\bullet-}$ (617 nm) radicals.[45,46] These data indicated simultaneous electrochemical and chemical reactions in the Li−S system, in agreement with the expected sulfur chemistry. Additional observations showed that the S_8^{2-} and S_4^{2-} levels in the CNTs electrodes were altered only slightly, which agree with the decreased I_{pa}/I_{pc} and ΔE_v values obtained from the data in Figure 2. Interestingly, compared with that of the CNTs/TPP electrode, the concentration of S_8^{2-} species in the CNTs/TFPP electrode was found to be higher, whereas the S_4^{2-} species concentration was lower during the discharge process. Considering the results of the EIS, H-type, and XPS analyses above, it appears that strong chemical interactions between the TFPP and LiPSs not only modify the kinetics of the electrochemical processes in the electrolyte, but also promote the formation of short-chain clusters (Li_2S_x, x = 1, 2, 3, and 4) at the interface during the charge−discharge process.

In our prior work, the lithiation reaction was found to correlate with the highest occupied and lowest unoccupied

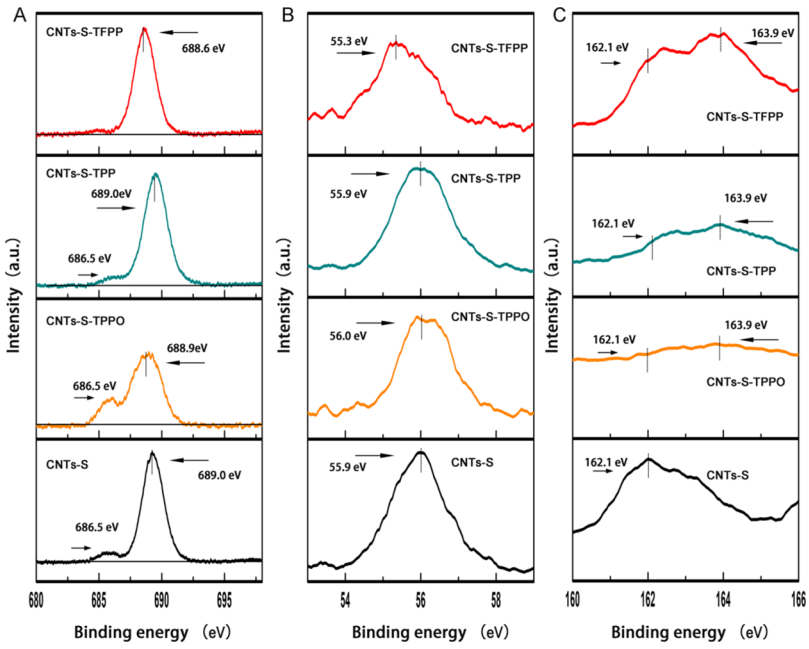

Figure 4. Study of chemical interactions between small molecules and LiPSs. (A) F 1s, (B) Li 1s, and (C) S 2p XPS spectra of CNTs/S/TFPP, CNTs/S/TPP, CNTs/S/TPPO, and CNTs/S.

DOI: 10.1021/acsami.9b10049
ACS Appl. Mater. Interfaces 2019, 11, 29978−29984

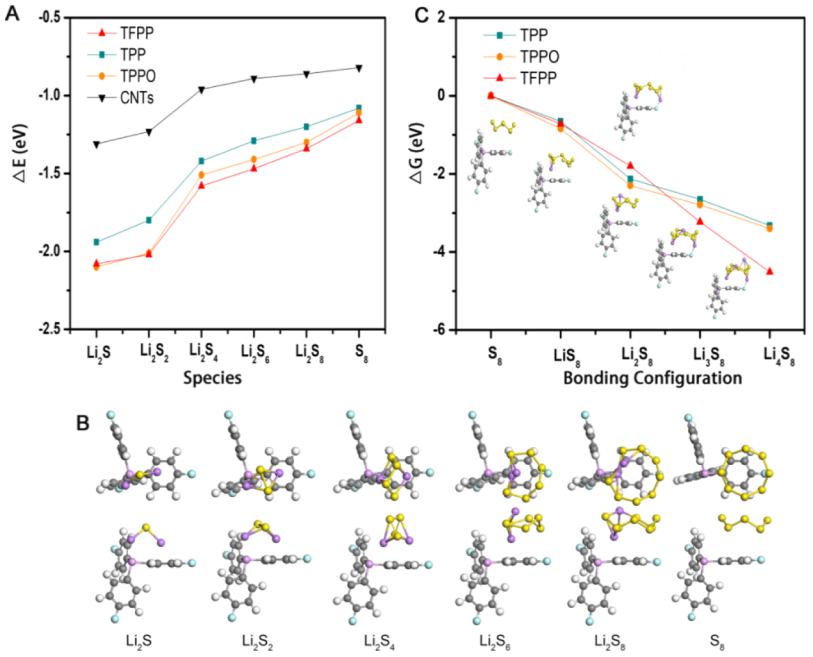

Figure 5. The effect of small molecule on lithiation reaction. (A) Calculated adsorption energy diagram of LiPSs interacting with TPP, TPPO, TFPP, and CNTs. (B) Schematic top (up) and side (front) views of optimal adsorption sites between LiPSs and TFPP. The carbon, hydrogen, oxygen, fluorine, phosphorus, lithium, and sulfur elements were represented by grey, white, red, cyan, lavender, purple, and yellow, respectively. (C) Binding energies and optimal configurations of intact and decomposed Li_2S_8.

molecular orbitals and the energy levels of TPP, TPPO, and TFPP.[47] Thus, a systemic theoretical study of lithium storage properties was performed, using a first principles method, and the resulting structures and frontier orbitals are presented in Figure S8. The energy values associated with the adsorption of LiPSs composites at various lithiation states during interactions with TPP, TPPO, TFPP, and the CNTs were examined by considering different initial configurations, and the associated energy diagrams and optimal adsorption geometries are provided in Figure 5A,B. It is apparent that the TFPP molecules exhibit the strongest binding performance. In the case of unlithiated S_8 adsorption, the cluster was parallel to one phenyl plane with a vertical range of 3.46 Å, and there were little or no effects on the cluster structures, with very few electrons transferred from the cluster to the TFPP molecule.

At the onset of lithiation, the adsorption strength between the LiPSs and TFPP molecules was enhanced to some extent, thus reducing the distance between S atoms and TFPP molecules and increasing the transfer of valence electrons. This led to strong ionic bonding and enhanced the anchoring effect. The stable configurations for LiPSs attached to TFPP demonstrate that the LiPSs compounds were closest to the P atoms of the TFPP. In particular, the intermediate state (Li_2S_4) was adsorbed perpendicular to the phenyl plane, whereas the initial states (Li_2S_8 and Li_2S_6) were anchored almost parallel to the phenyl plane (Figure 5B). In the case of pristine CNTs, there was minimal electron transfer between the LiPSs and the substrate, and the interaction between the two substances was due to physical adsorption via van der Waals forces. Stronger interactions would be expected to promote the formation of short-chain (Li_2S_x, x = 1, 2, 3, and 4) clusters and accelerate the conversion reaction during the charge−discharge process. These effects are reflected by the R_i of the cathode with TFPP as the mediator, as determined from the previous EIS data in Figure 3, as well as the results of in situ UV−visible spectroscopic analysis of the CNTs/TFPP electrode in Figure S7.

Prior research had shown that weak physical interactions between active LiPSs and various conducting scaffolds (such as graphene and CNTs) affect the rate cycling ability and increase electrode polarization, impeding the rapid, steady cycling performance expected from Li−S batteries.[48] Therefore, in the present work, the interactions of LiPSs with TFPP were assessed based on the atomistic thermodynamics of intact and decomposed LiPSs. In particular, two possible decomposition routes were compared, involving Li_2S_8 and LiS_8Li. Figure 5C provides the binding energies and optimal configurations for both intact and decomposed Li_2S_8. The adsorption energy differences between the intact form and both decomposed configurations were positive, demonstrating that an additional energy input is needed to decompose the intact Li_2S_8. Thus, adsorption of the LiS_8Li cluster structure on the CNTs/S/TFPP proceeds preferentially, promoting the formation of Li_2S_4 products. This conclusion is consistent with the previous in situ UV−visible spectroscopy data in Figure S7. It is apparent that the anchoring effects of TFPP primarily originate from chemical interactions between the LiPSs species and F and P atoms in the TFPP, and that these interactions are sufficient to overcome the weak adsorption of LiPSs on the CNTs. Additionally, it is likely that O atoms in TPPO molecules modify the P−S bonds, which also decreases the adsorption of the LiPSs. The strengths of the bonding of the LiPSs to the mediators decrease in the order of TFPP > TPP > TPPO. The mediators work to prevent the LiPSs from dissolving into the electrolyte, thereby improving the cycling performance of the Li−S batteries.

3. CONCLUSIONS

This work demonstrated a small molecular design strategy by introducing three small molecules acting as interfacial

DOI: 10.1021/acsami.9b10049
ACS Appl. Mater. Interfaces 2019, 11, 29978−29984

mediators to the cathodes of Li−S batteries. Batteries employing TFPP as a cathode mediator exhibited excellent cycling stability and high capacity retention. An experimental unit delivered a reversible specific capacity over 1000 cycles at 5 C with an ultralow capacity degradation of 0.042% per cycle. Furthermore, EIS, XPS, and in situ UV−visible spectroscopy data together with theoretical calculations confirmed that this outstanding performance can be ascribed to chemical interactions between LiPSs and F, P atoms in the TFPP. These interactions suppress the shuttle effect and enhance the kinetics during liquid−liquid phase transition, while also promoting the initial activation of liquid−solid transformations at the interface. Employing this small molecular design strategy to improve battery performance offers a promising avenue for in-depth mechanistic investigations of mediator-controlled kinetics as well as structure−performance relationships.

■ ASSOCIATED CONTENT

Supporting Information

The Supporting Information is available free of charge on the ACS Publications website at DOI: 10.1021/acsami.9b10049.

Complete experimental detail; rate performance of CNTs-S-TFPP with different mass ratio of TFPP; CV plots; I_{pa}/I_{pc} and voltage hysteresis of the four cathodes; galvanostatic discharge-charge plots; voltage hysteresis of the four cathodes; characteristics of various carbon-sulfur composites reported in literature; F 1s spectrum of CNTs-S-TFPP with different binders; digital photographs of the H-type simulation electrolytic cell CV test; schematic diagram of in-situ ultraviolet measurement; in situ UV-visible absorption spectra; and molecule configurations for LiPSs composites at various lithiation states (PDF)

■ AUTHOR INFORMATION

Corresponding Author

*E-mail: yang201079@126.com.

ORCID

Guoyong Fang: 0000-0001-6817-3790

Zhi Yang: 0000-0002-9265-5041

Notes

The authors declare no competing financial interest.

■ ACKNOWLEDGMENTS

The work was supported in part by grants from National Natural Science Foundation of China (21875166, 51741207, 51572197, and 21475096) and Natural Science Foundation of Zhejiang Province for Distinguished Young Scholars (LR18E020001). We are grateful to Chongqing Qindong Tech. Co. Ltd. for scientific computing assistance. We thank Michael D. Judge, from Liwen Bianji, Edanz Editing China for editing the English text of a draft of this manuscript.

■ REFERENCES

(1) Yu, M.; Ma, J.; Song, H.; Wang, A.; Tian, F.; Wang, Y.; Qiu, H.; Wang, R. Atomic layer deposited TiO_2 on a nitrogen-doped graphene/sulfur electrode for high performance lithium−sulfur batteries. *Energy Environ. Sci.* **2016**, *9*, 1495−1503.

(2) Chen, K.; Sun, Z.; Fang, R.; Shi, Y.; Cheng, H.-M.; Li, F. Metal−Organic Frameworks (MOFs)-Derived Nitrogen-Doped Porous Carbon Anchored on Graphene with Multifunctional Effects for Lithium−Sulfur Batteries. *Adv. Funct. Mater.* **2018**, *28*, 1707592.

(3) Li, G.; Gao, Y.; He, X.; Huang, Q.; Chen, S.; Kim, S. H.; Wang, D. Organosulfide-plasticized solid-electrolyte interphase layer enables stable lithium metal anodes for long-cycle lithium-sulfur batteries. *Nat. Commun.* **2017**, *8*, 850.

(4) Li, G.; Huang, Q.; He, X.; Gao, Y.; Wang, D.; Kim, S. H.; Wang, D. Self-Formed Hybrid Interphase Layer on Lithium Metal for High-Performance Lithium−Sulfur Batteries. *ACS Nano* **2018**, *12*, 1500−1507.

(5) Fang, R.; Zhao, S.; Sun, Z.; Wang, D.-W.; Cheng, H.-M.; Li, F. More Reliable Lithium-Sulfur Batteries: Status, Solutions and Prospects. *Adv. Mater.* **2017**, *29*, 1606823.

(6) Zhang, Z.-W.; Peng, H.-J.; Zhao, M.; Huang, J.-Q. Heterogeneous/Homogeneous Mediators for High-Energy-Density Lithium-Sulfur Batteries: Progress and Prospects. *Adv. Funct. Mater.* **2018**, *28*, 1707536.

(7) Seh, Z. W.; Sun, Y.; Zhang, Q.; Cui, Y. Designing high-energy lithium-sulfur batteries. *Chem. Soc. Rev.* **2016**, *45*, 5605−5634.

(8) Xiong, S.; Regula, M.; Wang, D.; Song, J. Toward Better Lithium−Sulfur Batteries: Functional Non-aqueous Liquid Electrolytes. *Electrochem. Energy Rev.* **2018**, *1*, 388−402.

(9) Liu, M.; Zhou, D.; He, Y.-B.; Fu, Y.; Qin, X.; Miao, C.; Du, H.; Li, B.; Yang, Q.-H.; Lin, Z.; Zhao, T. S.; Kang, F. Novel gel polymer electrolyte for high-performance lithium−sulfur batteries. *Nano Energy* **2016**, *22*, 278−289.

(10) Ruan, C.; Yang, Z.; Nie, H.; Zhou, X.; Guo, Z.; Wang, L.; Ding, X.; Chen, X. a.; Huang, S. Three-dimensional sp^2 carbon networks prepared by ultrahigh temperature treatment for ultrafast lithium-sulfur batteries. *Nanoscale* **2018**, *10*, 10999−11005.

(11) Chen, T.; Cheng, B.; Zhu, G.; Chen, R.; Hu, Y.; Ma, L.; Lv, H.; Wang, Y.; Liang, J.; Tie, Z.; Jin, Z.; Liu, J. Highly Efficient Retention of Polysulfides in "Sea Urchin"-Like Carbon Nanotube/Nanopolyhedra Superstructures as Cathode Material for Ultralong-Life Lithium-Sulfur Batteries. *Nano Lett.* **2017**, *17*, 437−444.

(12) Wang, L.; Yang, Z.; Nie, H.; Gu, C.; Hua, W.; Xu, X.; Chen, X. a.; Chen, Y.; Huang, S. A lightweight multifunctional interlayer of sulfur−nitrogen dual-doped graphene for ultrafast, long-life lithium−sulfur batteries. *J. Mater. Chem. A* **2016**, *4*, 15343−15352.

(13) Liu, X.; Xu, N.; Qian, T.; Liu, J.; Shen, X.; Yan, C. Stabilized Lithium-Sulfur Batteries by Covalently Binding Sulfur onto the Thiol-Terminated Polymeric Matrices. *Small* **2017**, *13*, 1702014.

(14) Sun, Z.; Zhang, J.; Yin, L.; Hu, G.; Fang, R.; Cheng, H.-M.; Li, F. Conductive porous vanadium nitride/graphene composite as chemical anchor of polysulfides for lithium-sulfur batteries. *Nat. Commun.* **2017**, *8*, 14627.

(15) Fang, R.; Zhao, S.; Hou, P.; Cheng, M.; Wang, S.; Cheng, H.-M.; Liu, C.; Li, F. 3D Interconnected Electrode Materials with Ultrahigh Areal Sulfur Loading for Li−S Batteries. *Adv. Mater.* **2016**, *28*, 3374−3382.

(16) Chen, S.; Yu, Z.; Gordin, M. L.; Yi, R.; Song, J.; Wang, D. A Fluorinated Ether Electrolyte Enabled High Performance Prelithiated Graphite/Sulfur Batteries. *ACS Appl. Mater. Interfaces* **2017**, *9*, 6959−6966.

(17) Xiao, Z.; Yang, Z.; Wang, L.; Nie, H.; Zhong, M. e.; Lai, Q.; Xu, X.; Zhang, L.; Huang, S. A Lightweight TiO_2/Graphene Interlayer, Applied as a Highly Effective Polysulfide Absorbent for Fast, Long-Life Lithium-Sulfur Batteries. *Adv. Mater.* **2015**, *27*, 2891−2898.

(18) Hua, W.; Yang, Z.; Nie, H.; Li, Z.; Yang, J.; Guo, Z.; Ruan, C.; Chen, X. a.; Huang, S. Polysulfide-Scission Reagents for the Suppression of the Shuttle Effect in Lithium-Sulfur Batteries. *ACS Nano* **2017**, *11*, 2209−2218.

(19) Guo, Z.; Nie, H.; Yang, Z.; Hua, W.; Ruan, C.; Chan, D.; Ge, M.; Chen, X. a.; Huang, S. 3D CNTs/Graphene-S-Al_3Ni_2 Cathodes for High-Sulfur-Loading and Long-Life Lithium-Sulfur Batteries. *Adv. Sci.* **2018**, *5*, 1800026.

(20) Zhang, Q.; Wang, Y.; Seh, Z. W.; Fu, Z.; Zhang, R.; Cui, Y. Understanding the Anchoring Effect of Two-Dimensional Layered Materials for Lithium-Sulfur Batteries. *Nano Lett.* **2015**, *15*, 3780−3786.

(21) Lei, T.; Xie, Y.; Wang, X.; Miao, S.; Xiong, J.; Yan, C. TiO_2 Feather Duster as Effective Polysulfides Restrictor for Enhanced Electrochemical Kinetics in Lithium-Sulfur Batteries. *Small* **2017**, *13*, 170103.
(22) Liu, X.; Xu, N.; Qian, T.; Liu, J.; Shen, X.; Yan, C. High coulombic efficiency and high-rate capability lithium sulfur batteries with low-solubility lithium polysulfides by using alkylene radicals to covalently connect sulfur. *Nano Energy* **2017**, *41*, 758−764.
(23) Yuan, Z.; Peng, H.-J.; Hou, T.-Z.; Huang, J.-Q.; Chen, C.-M.; Wang, D.-W.; Cheng, X.-B.; Wei, F.; Zhang, Q. Powering Lithium−Sulfur Battery Performance by Propelling Polysulfide Redox at Sulfiphilic Hosts. *Nano Lett.* **2016**, *16*, 519−527.
(24) Li, G.; Liu, Z.; Huang, Q.; Gao, Y.; Regula, M.; Wang, D.; Chen, L.-Q.; Wang, D. Stable metal battery anodes enabled by polyethylenimine sponge hosts by way of electrokinetic effects. *Nat. Energy* **2018**, *3*, 1076−1083.
(25) Chen, S.; Wang, D.; Zhao, Y.; Wang, D. Superior Performance of a Lithium−Sulfur Battery Enabled by a Dimethyl Trisulfide Containing Electrolyte. *Small Methods* **2018**, *2*, 1800038.
(26) Peng, H.-J.; Huang, J.-Q.; Liu, X.-Y.; Cheng, X.-B.; Xu, W.-T.; Zhao, C.-Z.; Wei, F.; Zhang, Q. Healing High-Loading Sulfur Electrodes with Unprecedented Long Cycling Life: Spatial Heterogeneity Control. *J. Am. Chem. Soc.* **2017**, *139*, 8458−8466.
(27) Fan, L.; Li, M.; Li, X.; Xiao, W.; Chen, Z.; Lu, J. Interlayer Material Selection for Lithium-Sulfur Batteries. *Joule* **2019**, *3*, 361−386.
(28) Xiao, Y.; Zhang, X. D.; Zhu, Y. F.; Wang, P. F.; Yin, Y. X.; Yang, X.; Shi, J. L.; Liu, J.; Li, H.; Guo, X. D.; Zhong, B. H.; Guo, Y. G. Suppressing Manganese Dissolution via Exposing Stable {111} Facets for High-Performance Lithium-Ion Oxide Cathode. *Adv. Sci.* **2019**, *6*, 1801908.
(29) Qiu, L.; Xiang, W.; Tian, W.; Xu, C.-L.; Li, Y.-C.; Wu, Z.-G.; Chen, T.-R.; Jia, K.; Wang, D.; He, F.-R.; Guo, X.-D. Polyanion and cation co-doping stabilized Ni-rich Ni−Co−Al material as cathode with enhanced electrochemical performance for Li-ion battery. *Nano Energy* **2019**, *63*, 103818.
(30) Xiong, D.; Li, X.; Bai, Z.; Lu, S. Recent Advances in Layered Ti3C2Tx MXene for Electrochemical Energy Storage. *Small* **2018**, *14*, 1703419.
(31) Xiao, Y.; Wang, P.-F.; Yin, Y.-X.; Zhu, Y.-F.; Niu, Y.-B.; Zhang, X.-D.; Zhang, J.; Yu, X.; Guo, X.-D.; Zhong, B.-H.; Guo, Y.-G. Exposing {010} Active Facets by Multiple-Layer Oriented Stacking Nanosheets for High-Performance Capacitive Sodium-Ion Oxide Cathode. *Adv. Mater.* **2018**, *30*, 1803765.
(32) Jin, R.; Li, X.; Sun, Y.; Shan, H.; Fan, L.; Li, D.; Sun, X. Metal−Organic Frameworks-Derived Co2P@N-C@rGO with Dual Protection Layers for Improved Sodium Storage. *ACS Appl. Mater. Interfaces* **2018**, *10*, 14641−14648.
(33) Lang, S.-Y.; Xiao, R.-J.; Gu, L.; Guo, Y.-G.; Wen, R.; Wan, L.-J. Interfacial Mechanism in Lithium-Sulfur Batteries: How Salts Mediate the Structure Evolution and Dynamics. *J. Am. Chem. Soc.* **2018**, *140*, 8147−8155.
(34) Lang, S.-Y.; Shi, Y.; Guo, Y.-G.; Wen, R.; Wan, L.-J. High-Temperature Formation of a Functional Film at the Cathode/Electrolyte Interface in Lithium-Sulfur Batteries: An In Situ AFM Study. *Angew. Chem., Int. Ed.* **2017**, *56*, 14433−14437.
(35) Peng, H.-J.; Zhang, Z.-W.; Huang, J.-Q.; Zhang, G.; Xie, J.; Xu, W.-T.; Shi, J.-L.; Chen, X.; Cheng, X.-B.; Zhang, Q. A Cooperative Interface for Highly Efficient Lithium-Sulfur Batteries. *Adv. Mater.* **2016**, *28*, 9551−9558.
(36) Zhou, J.; Qian, T.; Xu, N.; Wang, M.; Ni, X.; Liu, X.; Shen, X.; Yan, C. Selenium-Doped Cathodes for Lithium-Organosulfur Batteries with Greatly Improved Volumetric Capacity and Coulombic Efficiency. *Adv. Mater.* **2017**, *29*, 1701294.
(37) Frignani, A.; Monticelli, C.; Tassinari, M.; Trabanelli, G.; Bard, A. J.; Faulkner, L.R. *Electrochemical Methods: Fundamentals and Applications*, 2nd ed.; Wiley: New York, 2001; 2002.
(38) Deng, Z.; Zhang, Z.; Lai, Y.; Liu, J.; Li, J.; Liu, Y. Electrochemical Impedance Spectroscopy Study of a Lithium/Sulfur Battery: Modeling and Analysis of Capacity Fading. *J. Electrochem. Soc.* **2013**, *160*, 553−558.
(39) Ni, X.; Qian, T.; Liu, X.; Xu, N.; Liu, J.; Yan, C. High Lithium Ion Conductivity LiF/GO Solid Electrolyte Interphase Inhibiting the Shuttle of Lithium Polysulfides in Long-Life Li-S Batteries. *Adv. Funct. Mater.* **2018**, *28*, 1706513.
(40) Zhang, X.-Q.; Cheng, X.-B.; Chen, X.; Yan, C.; Zhang, Q. Fluoroethylene Carbonate Additives to Render Uniform Li Deposits in Lithium Metal Batteries. *Adv. Funct. Mater.* **2017**, *27*, 1605989.
(41) Hou, T.-Z.; Xu, W.-T.; Chen, X.; Peng, H.-J.; Huang, J.-Q.; Zhang, Q. Lithium Bond Chemistry in Lithium−Sulfur Batteries. *Angew. Chem., Int. Ed.* **2017**, *56*, 8178−8182.
(42) Zeng, Y.; Li, X.; Zhang, X.; Zheng, S.; Meng, L. Insight into the nature of the interactions of furan and thiophene with hydrogen halides and lithium halides: ab initio and QTAIM studies. *J. Mol. Model.* **2011**, *17*, 2907−2918.
(43) Li, X.; Zeng, Y.; Zhang, X.; Zheng, S.; Meng, L. Insight into the lithium/hydrogen bonding in $(CH_2)_2$X...LiY/HY (X: C=CH_2, O, S; Y=F, Cl, Br) complexes. *J. Mol. Model.* **2011**, *17*, 757−767.
(44) Nguyen, T. M. P.; Sheng, X.; Ting, Y.-P.; Pehkonen, S. O. Biocorrosion of AISI 304 Stainless Steel by Desulfovibrio desulfuricans in Seawater. *Ind. Eng. Chem. Res.* **2008**, *47*, 4703−4711.
(45) Zou, Q.; Lu, Y.-C. Solvent-Dictated Lithium Sulfur Redox Reactions: An Operando UV-vis Spectroscopic Study. *J. Phys. Chem. Lett.* **2016**, *7*, 1518−1525.
(46) Zheng, D.; Qu, D.; Yang, X.-Q.; Yu, X.; Lee, H.-S.; Qu, D. Quantitative and Qualitative Determination of Polysulfide Species in the Electrolyte of a Lithium-Sulfur Battery using HPLC ESI/MS with One-Step Derivatization. *Adv. Energy Mater.* **2015**, *5*, 1401888.
(47) Lau, V. W.-h. L.; Moudrakovski, I.; Botari, T.; Weinberger, S.; Mesch, M. B.; Duppel, V.; Senker, J.; Blum, V.; Lotsch, B. V. Rational design of carbon nitride photocatalysts by identification of cyanamide defects as catalytically relevant sites. *Nat. Commun.* **2016**, *7*, 12165.
(48) Hou, T.-Z.; Xiang, C.; Peng, H.-J.; Huang, J.-Q.; Li, B.-Q.; Zhang, Q.; Li, B. Design Principles for Heteroatom-Doped Nanocarbon to Achieve Strong Anchoring of Polysulfides for Lithium-Sulfur Batteries. *Small* **2016**, *12*, 3283.

DOI: 10.1021/acsami.9b10049
ACS Appl. Mater. Interfaces 2019, 11, 29978−29984